COMPARATIVE RISK-BASED SEISMIC ASSESSMENT OF 1970S VS MODERN TALL STEEL MOMENT FRAMES

Carlos Molina Hutt[1], Tiziana Rossetto[2] and Gregory G. Deierlein[3]

[1]Civil Engineering, University of British Columbia, Vancouver, BC
[2]Civil, Environmental and Geomatic Engineering, University College London, London, UK
[3]Civil and Environmental Engineering, Stanford University, Stanford, CA

This study benchmarks the performance of older existing tall steel moment resisting frame buildings designed following historic code-prescriptive requirements (1973 Uniform Building Code) against modern design standards (2015 International Building Code). The comparison is based on seismic risk assessments of alternative designs of a 50-story archetype office building, located at a site in San Francisco, CA. The mean annual frequency collapse risk of the 1973 building is 28 times greater than the equivalent 2015 building (28×10^{-4} versus 1×10^{-4}), or approximately 13% versus 0.5% probability of collapse in 50 years. The average annual economic loss (based on cost of repair) is 65% higher for the 1973 as compared to the 2015 building (0.66% versus 0.40% of building replacement cost). The average annual downtime to re-occupancy for the 1973 building is 72% longer (8.1 vs 4.7 days) and to functional recovery is about 100% longer (10.4 vs 5.0 days). Building performance evaluations at the design basis earthquake (DBE) and the maximum considered earthquake (MCE) shaking intensities further suggest that 1970s tall steel moment frames have much higher risks of collapse under extreme ground motions and risks of damage and building closure in moderate earthquakes. Furthermore, while modern building code requirements provide acceptable seismic collapse safety, they do not necessarily ensure a level of damage control to assure a swift recovery after a damaging earthquake due to extensive downtime. A set of vulnerability functions are proposed for both archetype buildings considered in the assessment.

KEYWORDS

steel moment resisting frames, tall buildings, seismic risk-based assessment, loss, downtime, collapse, vulnerability functions.

INTRODUCTION

Tall buildings play an important role in the socio-economic activity of major metropolitan areas in the United States and other countries. Tall buildings house many businesses or residents, which raises concerns that damage to these buildings has the potential to affect a large number of people. Furthermore, severe damage to even a single tall building can have significant consequences on surrounding areas. Events such as the Canterbury earthquake in 2011 have highlighted the impact of hazardous buildings on the business continuity of districts where tall buildings are clustered together. For example, following the 2011 Christchurch earthquake, the 26-story Hotel Grand Chancellor sustained severe damage, where the risk of collapse from aftershocks prompted authorities to set up a cordon around the building with a 90 meter radius, roughly equal to the height of the damaged building [1]. Thus, compounding the direct economic loss associated with the damaged hotel building, there were significant indirect losses attributed to business disruption in surrounding buildings.

Until recently, tall buildings have generally been designed following prescriptive force-based elastic analysis approaches [2] that do not provide an explicit assessment of expected performance to major earthquakes. This is in spite of the fact that prescriptive elastic design approaches may not adequately account for the unique attributes of tall buildings, most notably the contribution of long period response and higher mode effects associated with slender aspect ratios [3]. As a result, several jurisdictions in areas of high seismicity in the western United States (e.g. Los Angeles and San Francisco) have adopted performance-based design approaches, which require the use of nonlinear response history analyses to evaluate response under severe (maximum considered earthquake, MCE) ground motions. While these approaches generally provide more reliability in terms of building safety, they usually stop short of employing explicit performance-based methods to assess the risk of damage, economic losses, and downtime. More importantly, little is known about the seismic performance of older existing tall buildings that were designed prior to the adoption of modern design approaches [4].

A major concern in earthquake disaster resilience is the potentially large risks posed by existing tall buildings that were designed by outdated building codes. These include many steel moment frame buildings, constructed during the late 1960s through mid-1990s with the type of welded connections that experienced sudden brittle fractures during the 1994 Northridge earthquake. Many buildings of this era were designed and constructed without capacity design principles to protect against story mechanisms, without code mandated seismic drift limits, and with lower base shear strengths than those specified in current codes. Compounding these deficiencies are new seismological data and models indicating that earthquake ground motion hazards at long periods, which can affect tall buildings, may be larger than previously thought [5]. Finally, there is growing realization that even in the best of circumstances, minimum building code requirements may not ensure a level of damage control to ensure the seismic resilience of communities.

For some types of buildings, such as unreinforced masonry structures, the risks are so large, that mandatory laws have been enacted to assess and retrofit the buildings. However, in other cases, such as with non-ductile concrete buildings or older tall steel buildings, the risks and mitigation strategies are not as straightforward. The goal of this study is to benchmark against modern designs the performance of older seismically vulnerable tall steel moment resisting frame (MRF) buildings, which constitute a significant portion of tall buildings constructed between 1960 and 1990 [4] in San Francisco, Los Angeles and other high seismic regions of the western United States. The comparison is focused on risk metrics that can help inform policy and decision making, developed by means of risk-based assessments of alternative designs of a 50-story archetype office building located at a site in San Francisco, CA: a steel MRF designed following the requirements of the 1973 Uniform Building Code (UBC) [6], hereinafter referred to as the 1973 archetype, and a steel MRF designed following the 2015 International Building Code (IBC) [7], hereinafter referred to as the 2015 archetype.

The 1973 archetype is intended to represent a plausible design from the mid-1970s to the mid-1980s. Characteristics of its design are based on an inventory and review of design drawings of existing tall buildings in San Francisco from that era, which revealed at least 10 steel moment-resisting frame buildings taller than 40 stories in height [4]. The 2015 archetype is a building of the same geometry and occupancy as the 1973 archetype, but designed following modern building code requirements. The 2015 archetype is not intended to represent modern construction practice, which would likely adopt a reinforced concrete shear wall or steel braced frame system, but rather it intends to serve as a performance benchmark of the same lateral force resisting system designed to modern standards. These evaluations and comparison of the two archetypes are useful to assess compliance of the designs with the life-safety objective of the code under MCE intensity motions and an understanding of expected performance at other earthquake intensities.

METHODOLOGY

A risk-based assessment consists of the evaluation of a number of intensity-based performance assessments under a range of ground motion intensity levels which are then combined with the ground motion hazard curve to provide the annual rates of exceedance of a performance measure, e.g. economic loss [8]. The technical basis of this methodology was developed by the Pacific Earthquake Engineering Research (PEER) center and applies the total probability theorem to predict earthquake consequences in terms of the probability of incurring a particular value of a performance measure [9]. Under this framework, performance is computed by integrating (1) the probability of incurring an earthquake of different intensities over all possible intensities, (2) the probability of incurring a certain building response (e.g. drift, acceleration, etc.) given an intensity of ground shaking, and (3) the probability of incurring certain damage and consequences given a value of building response [10].

The performance assessment methodology follows a Multiple Stripe Analysis (MSA) approach, where the performance is assessed at eight seismic hazard intensity levels. Nonlinear dynamic analyses are conducted with ground motion suites representative of each intensity, and results of the analyses are used to assess structural performance, associated damage and consequence (loss and downtime). The analysis results are then linked back to probabilistic seismic hazard data, which enables calculating a range of risk metrics, e.g. collapse risk.

Referring to Figure 1, the building assessment methodology entails the following steps: (1) design of the archetype buildings based on a database of the existing tall building stock and selection of a representative site in the case study city; (2) quantification of the seismic hazard at the representative site and selection of hazard consistent ground motions; (3) development of numerical models for structural and building performance simulations; (4) integration of results with probabilistic seismic hazard data to develop risk metrics and vulnerability functions.

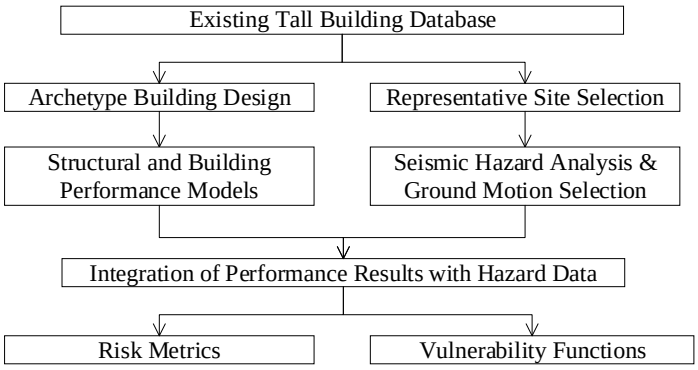

Figure 1. Schematic diagram of risk-based seismic assessment methodology.

ARCHETYPE BUILDING DESIGN

The SEAONC Committee on Performance-Based Seismic Design (PBSD) of Tall Buildings developed a database of buildings in San Francisco that are taller than 50 m (~160 ft). The database tabulates building characteristics by location, height, number of stories, year built, and lateral system type. Analysis of this database by [4] revealed that steel MRFs are the most prevalent lateral resisting system in pre-1990s construction for buildings greater than 35 stories in height. Figure 2 depicts the locations of buildings that are greater than 35 stories and which the existing tall building database identifies as steel MRF. The majority of these buildings are clustered in the downtown area, located approximately 14 km from the San Andreas Fault and 16 km from the Hayward Fault. A representative site is selected in close proximity to the existing tall buildings with soil properties consistent with ASCE 7 Site Class D [11].

The 1973 archetype selected for this study is regular in plan and represents the state of design and construction practice for tall buildings from the mid-1970s to the mid-1980s. The building has a commercial office occupancy with two levels for mechanical equipment, one at mid-height, and one at the top floor. The building enclosure is assumed to be composed of precast concrete panels and glass windows, a floor system composed of concrete slab 76.2 mm (3 in.) over metal deck 63.5 mm (2.5 in.) supported by steel beams of ASTM A36 [248 MPa (36 ksi)], and steel columns of ASTM A572 [345MPa (50 ksi)]. The lateral resisting system of the building is a space MRF with wide flange beams, built up box columns, and welded beam-column connections. Typical story heights are 3.8 m (12.5 ft), except at the lobby where the height is 6.1 m (20 ft). The overall height of the structure is 192.8 m (632.5 ft) above grade, and the building width is 51.2 m (168 ft), consisting of 6 bays of 8.5 m (28 ft) in each direction. The 2015 archetype is consistent with the 1973 archetype, except that it employs a perimeter frame as opposed to a space frame, as shown in Figure 3, where MF denotes moment resisting frame.

Figure 2. Rendering of tall buildings constructed from 1960 to 1994 in downtown San Francisco, CA classified according to structural system. Adapted from [12].

The 1973 archetype is designed in accordance with the 1973 UBC and the SEAOC Bluebook of 1973 [13], which was commonly employed to supplement minimum design requirements. Based on discussions with engineers knowledgeable of the design practice of the time [14], even though 1973 UBC did not specify drift limits, design offices would have implemented drift limits established by their firm's practice or those obtained from the Bluebook. In this paper, the drift limit recommendations from Appendix D of the Bluebook for buildings taller than 13 stories are used, equal to story drift ratios of 0.0025 for wind and 0.005 for seismic (based on elastic design drifts). Modern code requirements result in a slightly more stringent seismic drift limit of approximately 0.004. Note that the 0.004 value, based on elastic code-level forces, corresponds to an inelastic story drift limit of 0.020, where a deflection amplification factor of C_d equal to 5.5 is used to convert elastic to inelastic drifts for special steel MRF [11]. Although the limiting drift ratios in the 1973 archetype are similar to those in current standards, the resulting stiffness is less because the seismic design forces are larger in modern building codes. Per the 1973 UBC design standards, the required effective wind base shear is 1.8% and the effective seismic base shear is 2.0%, whereas per 2015 IBC requirements, the effective wind base shear is 4.3% and the overall effective seismic base shear is 3.7%. The 2015 IBC seismic design base shear is controlled by minimum base shear requirements, which were not included in the 1970s design regulations. Furthermore, there are a number of additional seismic design considerations in current standards that were not present in the 1970s, including: (1) use of response spectrum analysis method as opposed to equivalent lateral force procedures; (2) consideration of lateral forces acting simultaneously in both building directions; (3) minimum base shear requirements (scaling of forces and displacements); (4) p-delta effects (scaling of forces and displacements); (5) consideration of accidental torsion and vertical and horizontal irregularities; (6) strong column weak beam requirements; (7) panel zone design checks; (8) capacity design principles; and (9) prequalified seismic connection details.

It is well established that changes in commonly used weld processes during the mid-1960s led to welds with low toughness, as evidenced by weld fractures observed in the 1994 Northridge earthquake [15]. Therefore, it is assumed that fracture-prone pre-Northridge moment connections are present in the 1973 archetype. In addition, since the panel zone model proposed by Krawinkler was not developed until 1978 [16] and strong column-weak beam requirements were not introduced in the UBC provisions until 1988 [17], the 1973 archetype does not include consideration of panel zone flexibility or strong column-weak beam principles. While these requirements were not present in the 1973 UBC, the use of large boxed columns, observed in numerous existing building drawings, resulted in designs that generally complied with modern standards, particularly near the base of the building.

Typical member types and connection details for the 1973 archetype are selected based on trends observed in drawings of existing tall steel MRF buildings. Accordingly, built-up box columns (denoted R in Figure 3) and rolled wide flange beams are selected for the 1973 archetype. For the modern archetype building design, built-up I sections (denoted I in Figure 3) are selected for the columns and wide flange sections are selected for the beams, with both assumed to have the same steel grade as the 1973 archetype. A summary of typical design section sizes is shown in Figure 3. The lateral resisting system for the 1973 archetype consists of 7 frames in each direction, whereas the 2015 archetype has only 2 frames in each direction (perimeter frame).

Column splices are typically located 1.2 m (4 ft) above the floor level at approximately every third floor. The 1973 archetype employs column splice connection details typical of the era, consisting of partial joint penetration welds of roughly half the thickness of the smaller section being connected. When subjected to tensile forces, these splices can only carry a fraction of the moment capacity and/or axial tension capacity of the smallest section size being connected. Furthermore, experimental tests on heavy steel section welded splices have illustrated sudden failures with limited ductility [18]. Based on this evidence, column splice failures are considered in the assessment.

For the 2015 archetype, pre-qualified Reduced Beam Section (RBS) moment connection details and column splices that develop the full capacity of the smaller size column are used. Therefore, premature fractures of the beam-column connections or column splices are not considered in the 2015 archetype analysis model. In the design of the 2015 archetype, beam sections were limited to those for which pre-qualified moment connection details are available. As a result, large strong-column weak beam ratios are observed in this design. While this may be an artifact of such design constraint, the resulting performance of the building is consistent with that targeted by modern seismic design codes, as will be discussed later.

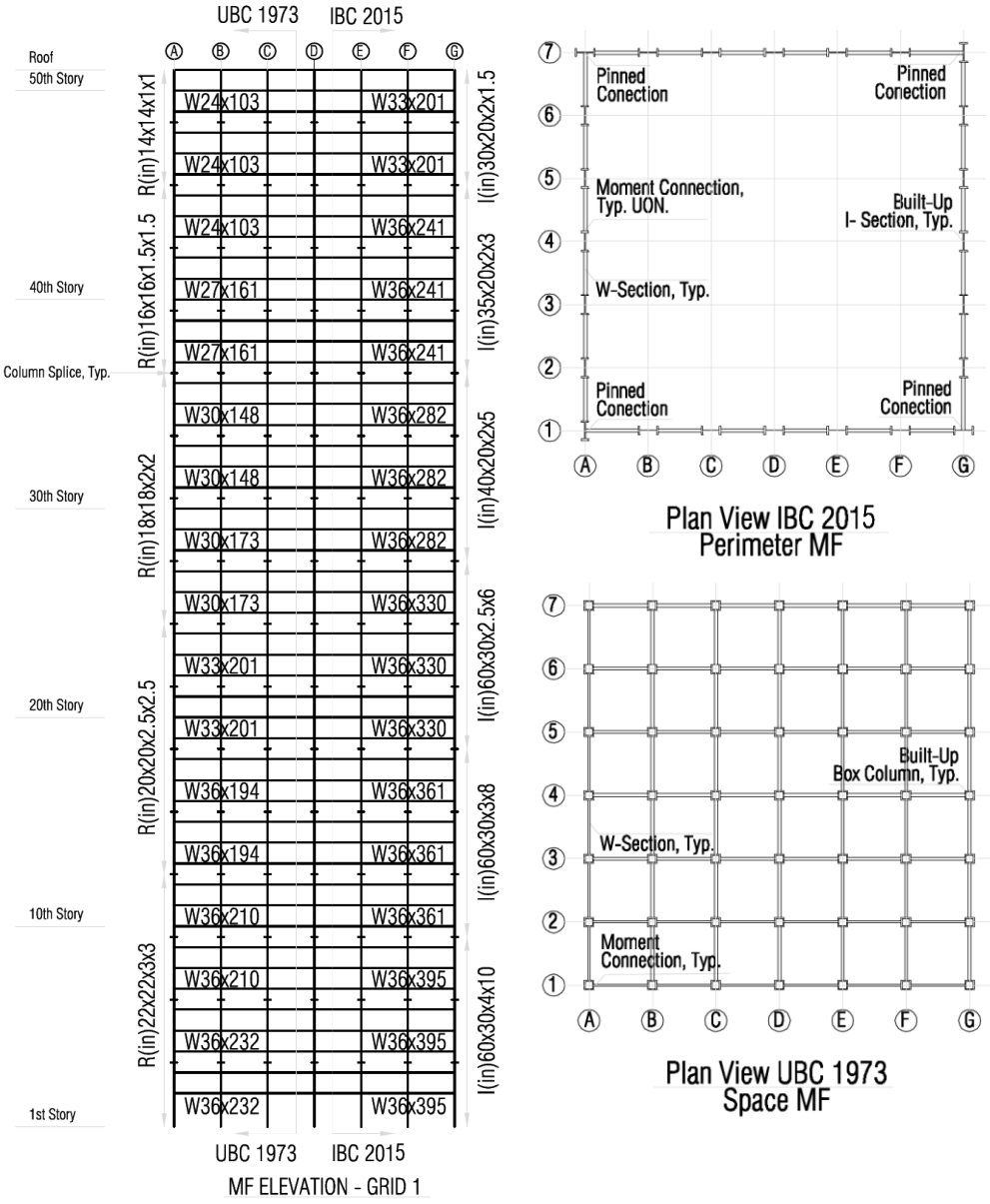

Figure 3. Elevation and plan views of the lateral resisting systems of the 1973 and 2015 archetype buildings.

The overall seismic weight of the 1973 archetype is 784,220 kN (176,300 kips), whereas the seismic weight of the 2015 archetype is 825,145 kN (185,500 kips). The 5% difference in seismic weight is a due to the larger steel member sizes in the 2015 archetype. Since the buildings are symmetric, the dynamic properties in each principal building direction are effectively identical. The dynamic properties of the archetypes in one of the principal building directions are summarized in Table 1. Three-dimensional models are used in the design of the archetype buildings; whereas two-dimensional models of a representative exterior frame are used for the nonlinear dynamic analyses to reduce computational time. The dynamic properties of the two-dimensional models (shown in parenthesis in Table 1) match closely those of the three-dimensional models.

The two-dimensional models fail to capture torsional and biaxial effects. Neglecting torsional effects is believed to have limited impact because the buildings considered present no significant torsional irregularity. Biaxial effects may underestimate column demands, particularly in the 1973 archetype, which consists of a space frame where all beam-to-column connections are moment resisting. In contrast, the evaluation of a single representative frame under extreme

loading also represents an inherent conservatism, particularly in the collapse risk estimates. In the case of the 1973 space frame archetype, the two-dimensional analysis fails to capture the redundancy associated with all beam-to-column connections having moment-resistance. In the case of the 2015 perimeter frame archetype, the two-dimensional analysis fails to capture the contributions of the gravity system to the overall response.

Table 1. Dynamic properties of the three-dimensional (and two-dimensional) archetypes in one of the principal building directions.

Mode	2015 IBC		1973 UBC	
	Period [s]	Effective / total mass [%]	Period [s]	Effective / total mass [%]
1	5.0 (5.1)	74.3 (75.0)	5.5 (5.7)	70.6 (71.3)
2	1.8 (2.0)	12.5 (15.2)	2.1 (2.2)	15.3 (15.6)
3	1.0 (1.2)	4.3 (4.4)	1.3 (1.3)	5.1 (5.2)
4	0.7 (0.9)	2.5 (2.1)	0.8 (0.9)	3.1 (3.0)
5	0.6 (0.7)	1.2 (0.9)	0.7 (0.7)	1.6 (1.5)

SEISMIC HAZARD AND GROUND MOTION SELECTION

Probabilistic Seismic Hazard Analysis (PSHA) enables the calculation of hazard curves, which express the annual rate of exceedance of ground motion parameters, such as the spectral acceleration (SA) at a selected period, at a particular site, considering the risk from all possible seismic sources. In a MSA, structural assessments are performed at a series of ground motion intensities spanning from high to low probability of occurrence. The upper and lower bound intensity levels considered should cover a range from negligible damage to complete loss. Referring to Figure 4, the minimum and maximum annual frequencies of exceedance (AFE) and corresponding SAs are selected based on the recommendation of [10] between AFE of 0.0002 to 0.04 with corresponding SAs based on the seismic hazard curve at the representative site in downtown San Francisco. United States Geological Survey (USGS) seismic hazard data is used in this study [19] to determine the seismic hazard curve for a 5 second period, which is close to the fundamental period of the archetype buildings.

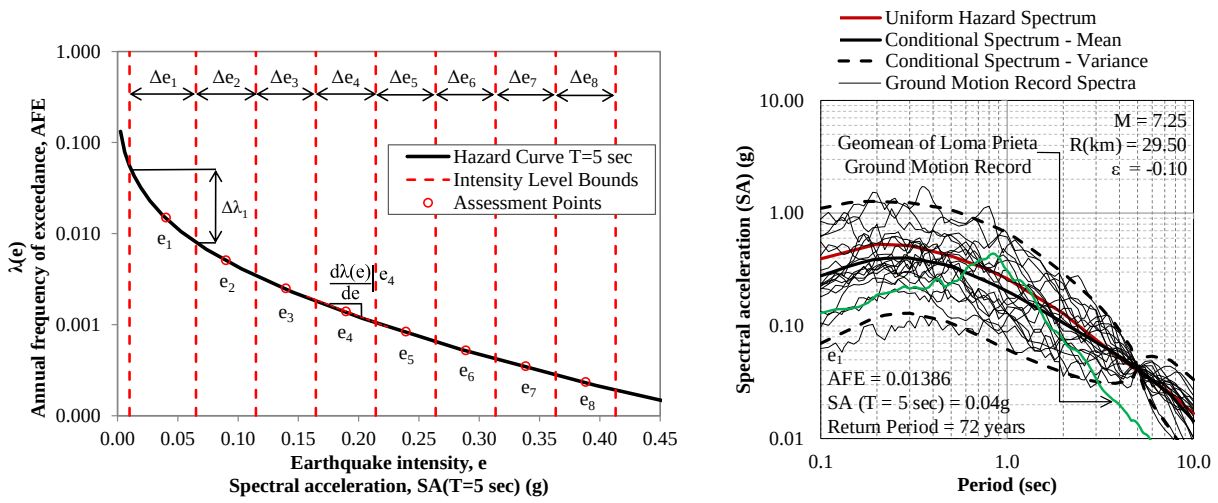

Figure 4. (a) Seismic hazard curve at the representative site in downtown San Francisco (Vs30=260m/s, T=5sec.) illustrating the earthquake ground motion intensities (e_i) considered in the risk-based assessment and (b) target conditional mean, variance, ground motion records and corresponding Uniform Hazard Spectrum for intensity level e_1 including SA, AFE, return periods and deaggregation data (M, R and ε), as well as geomean spectra of 1989 Loma Prieta ground motions recorded close to the representative site.

The lower bound SA is intended to represent a ground motion intensity level that does not result in significant damage to structural components whereas the upper bound SA is intended to represent a ground motion intensity beyond the level that triggers collapse. Once the bounds of spectral accelerations SA_{MIN} to SA_{MAX} are determined, the range is

split into eight equal intervals for assessment. The midpoint SA of each one of these intervals is then computed along with its corresponding AFE. This process is graphically illustrated in Figure 4, where the earthquake ground motion intensity intervals and the assessment points are denoted by Δe_i and e_i respectively.

Table 2. Summary seismic hazard data for the intensity levels considered in the risk-based assessment including SA at a 5 second period, AFE, return period and deaggregation data (M, R and ε).

Earthquake Ground Motion Intensity	SA (g)	AFE (1/year)	Return Period (years)	M (-)	R (km)	ε (-)
e_1	0.042	0.014	72	7.25	29.50	-0.10
e_2	0.089	0.005	199	7.50	19.90	0.30
e_3	0.140	0.0024	409	7.63	16.80	0.62
e_4	0.185	0.0014	712	7.70	15.60	0.85
e_5	0.220	0.00096	1039	7.73	15.10	1.01
e_6	0.284	0.00053	1898	7.78	14.40	1.25
e_7	0.314	0.00040	2475	7.80	14.10	1.35
e_8	0.370	0.00026	3899	7.82	13.80	1.51

In this study, the Conditional Spectrum (CS) method [20] is used to establish site- and structure-specific target spectra for selection and scaling of input ground motions for the structural dynamic analyses. The conditional spectrum is based on earthquake hazard deaggregation to identify the characteristic earthquake magnitude (M), distance (R) and epsilon (ε) for each intensity level, where ε is an indicator of spectral shape based on the difference between the computed spectral acceleration at a particular probability of exceedance and the spectral acceleration associated with the controlling magnitude and distance [20]. Table 2 summarizes the AFE, SA, M, R and ε associated with each earthquake ground motion intensity level based on USGS deaggregation data.

Based on the deaggregation data in Table 2, CS conditioned at the 5 second characteristic period of the building are developed [21] and suites of ground motions are then selected to collectively match the CS distribution using an algorithm developed by [22]. Figure 4b illustrates the target conditional mean spectrum and variance, as well as the ground motions selected for assessment for a sample intensity level with a 72 year return period. Also shown is a comparison with the corresponding uniform hazard spectrum (UHS) obtained from the USGS hazard data. Note that hazard data for periods longer than 5 seconds are not available from USGS, so these were determined from OpenSHA [23].

At each earthquake ground motion intensity, 20 records are selected to match the CS (mean and variance). Records are selected from the PEER NGA West 2 database [24]. The selection is limited to earthquake records with earthquake magnitudes greater than M5, source to site distances less than R=50 km, and scale factors less than five. Otherwise, no additional criteria are set for record selection concerning shear wave velocity profiles, pulses or other parameters. While the presence of ground motion pulses is not explicitly considered in the analysis, since the record selection is consistent with M, R and ε hazard deaggregation data, records with pulses are present in most ground motion suites, particularly at high earthquake ground motion intensities. The selected ground motions are input at the base of the structural model, which is assumed to have a rigid support at the base. Finally, as discussed in [25], since multiple CS and sets of records are used in the MSA approach, it is assumed that the single conditioning period of 5 seconds is sufficient to capture the full range of modal response in the analyses.

STRUCTURAL ANALYSIS MODEL

The nonlinear dynamic analysis models of the archetype buildings are capable of capturing the response of all structural elements that significantly contribute to the strength and stiffness of the system. The numerical model is developed for simulation in LS-DYNA [26]. LS-DYNA is a general purpose finite element code for analyzing the large deformation static and dynamic response of structures. The main solution methodology is based on explicit time integration. Component models representing the response of non-linear columns, beams and panel zones are calibrated against available experimental test data for validation so as to capture the full range of deterioration in strength and stiffness, from the onset of nonlinearity up to the point sideway instability. Two important modelling assumptions, which may underestimate the strength and stiffness estimates, include: (1) bare steel behavior (i.e. there is no

composite action between the beams and the concrete slab); (2) limited non-structural component contribution to the response (i.e. non-structural components are only implicitly accounted for through equivalent viscous damping).

Beams

For both archetype buildings, beams are modeled using a lumped plasticity approach. For the 2015 archetype, beams follow the modelling parameters recommended in [27] for RBS connections, which are based on a large database of experimental tests. These guidelines define the moment-rotation response as a function of the yield moment M_y, pre-capping plastic rotation θ_p, post-capping plastic rotation θ_{pc} and cumulative plastic rotation capacity Λ; all of which can be defined as a function of beam geometry and material properties. Figure 5a illustrates a comparison between the analytical and experimental [28] moment-rotation response of a beam with an RBS connection. For the 1973 archetype with pre-Northridge moment connections, the hysteretic response of the beams accounts for fracture based on ASCE 41 [29] recommendations. The modeling procedure is similar to that used for the 2015 archetype, but adjusted for non-RBS connections as outlined in [16] and introducing a plastic rotation threshold $\theta_{p\text{-}fract}$ at which fracture is set to occur in the connections as illustrated in Figure 5b.

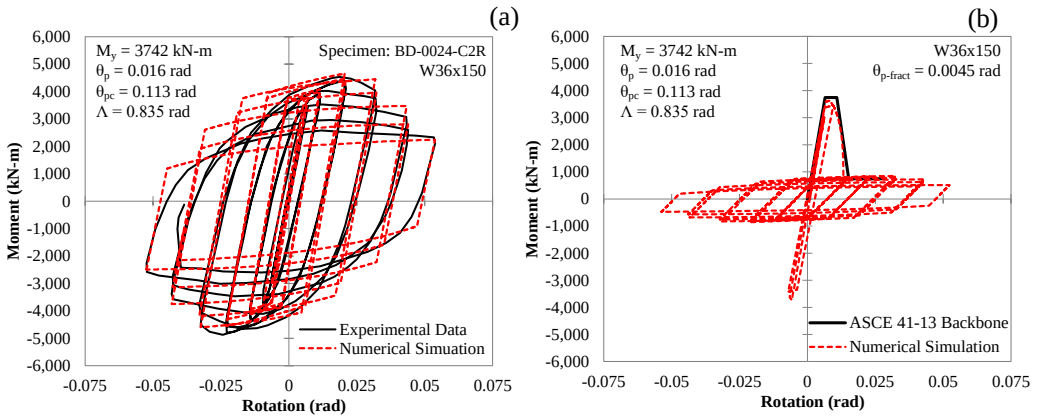

Figure 5. Hysteretic moment rotation response for (a) a sample RBS beam-to-column connection showing analytical versus experimental [28] results and (b) an identical section with fracture prone pre-Northridge connection behavior, modeled per ASCE 41 [29] recommendations.

Columns

Columns are modeled as lumped plasticity beam elements with yield surfaces capable of capturing interaction between bending moment and axial force. The yield surfaces at the hinge locations permit interaction between the bending moments and the axial force. A hinge forms when the following condition is satisfied:

$$\left|\frac{m}{M}\right|^{1.1} + \left|\frac{f}{F}\right|^{1.1} \geq 1 \quad (1)$$

where m is the bending moment demand, M is the bending strength, f is the axial force demand, and F represents the tensile strength (when f denotes tension) and compressive strength (when f denotes compression). The resulting yield surface is illustrated in Figure 8 for a sample column, including the axial load-bending moment time history response during a sample ground motion simulation.

Under low levels of axial load, the moment-rotation response of columns is similar to that of beams; however, under axial load-to-capacity ratios (ALR) greater than 0.2, the moment-rotation response experiences faster degradation. For the 1973 archetype, degradation parameters for the moment-rotation response under cyclic loads are calibrated based on experimental tests of tubular steel columns [30] in accordance with the guidelines for tubular hollow steel columns under varying levels of axial load [31]. The guidelines define the moment-rotation response not only as a function of the yield moment M_y, pre-capping plastic rotation θ_p, post-capping plastic rotation θ_{pc} and cumulative plastic rotation capacity Λ (based on cross section geometry and material properties), but also as a function of ALR. Figure 6a and

Figure 6b illustrate the component deterioration calibration results for two column samples with ALR of 0.1 and 0.3 respectively.

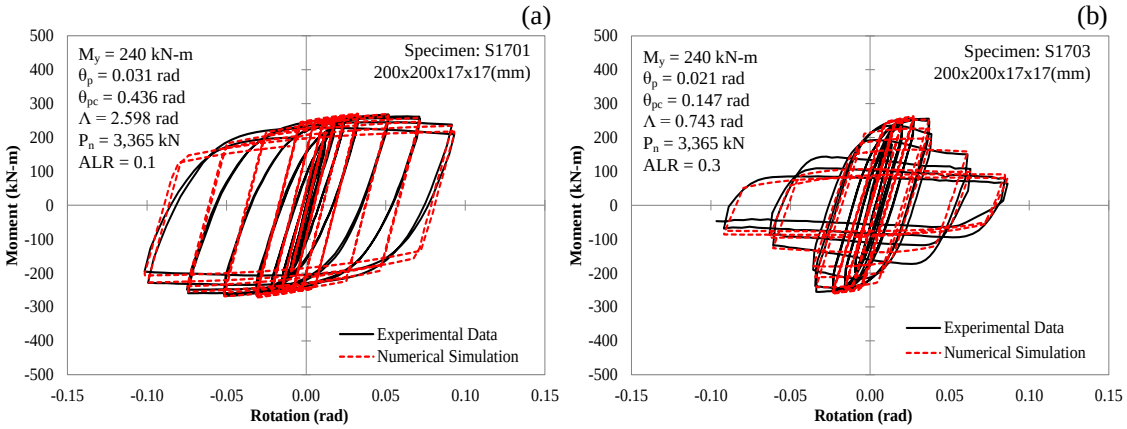

Figure 6. Sample analytical versus experimental [30] column moment-rotation hysteretic response under varying ALR: (a) 0.1 and (b) 0.3.

For the 1973 archetype, axial demands in the columns under expected gravity loads range from 20-30%, hence degradation parameters that account for ALR are considered. On the other hand, the 2015 archetype, the ALRs are low enough, in the range of 7-11%, such that degradation parameters for the moment-rotation response under cyclic loads are assumed to be equivalent to those outlined in [16] for steel beams.

Panel Zones

Panel zones are modeled using the Krawinkler model as outlined in [16], which incorporates an assembly of rigid links and rotational springs. The rigid links extend out to represent the full dimensions of the panel zone. The non-linear springs are calibrated to capture the trilinear shear force-deformation relation based on the geometric and material properties, assuming non-degrading panel zone shear behavior.

Column Splices

For the 1973 archetype, column splices are modeled by inserting lumped plasticity hinges with strengths equal to the expected splice under tension and/or bending. Splices are capable of reaching their expected capacity followed by brittle failure, with the intent to capture the limited ductility observed in experimental tests on heavy steel section welded splices observed by [18]. After splices reach their expected capacity, a residual strength of 20% is assumed. Full column capacity is assumed in compression since this is achieved by direct bearing. For the 2015 archetype, splices are assumed to develop the full capacity of the smallest section being connected, as required by modern building code standards.

Loads, Damping and Boundary Conditions

Analytical models are subject to ground motions in conjunction with expected gravity loads associated with the seismic weight of the structure. Seismic weight includes self-weight, superimposed dead load, and 25% of the unreduced live loads. For the 1973 archetype (space frame), the seismic mass (weight) stabilized by each frame is approximately equal to the tributary gravity load carried by the frame, whereas for the 2015 archetype (perimeter frame), the seismic mass for each perimeter frame is much greater than its tributary gravity load. Therefore, a leaning column is included in the 2015 archetype model to capture the p-delta effects from the seismic mass that is not tributary to the frame. A fixed base is assumed at ground level and 2.5% of critical viscous damping is assumed in the analysis [3]. The damping model used in the analysis provides constant 2.5% damping at a period range from 1 to 10 seconds.

Simulated versus Measured Response Data

To check whether the response of the 1973 archetype is representative of the existing tall building stock, its response is compared to that of the Chevron Building, an instrumented 42-story steel MRF building in downtown San Francisco, whose response was recorded during the 1989 Loma Prieta earthquake (Center of Engineering Strong Motion Data ID 1446 [32]). Construction of the Chevron building was completed in 1975, hence its design is believed to be consistent with the requirements of the 1973 UBC. With an overall height of 167 m (550 ft) and rectangular plan measuring 24 m (79 ft) by 46 m (151 ft), the Chevron building had measured vibration periods of 5.4, 1.8 and 1.1 seconds in the short building direction, and 5.1, 1.7 and 1.0 seconds in the long building direction [33]. Thus, these are similar to the calculated periods of the 1973 archetype, reported previously in Table 1.

The geomean spectra of the acceleration time history recorded during Loma Prieta earthquake at the base of the Chevron Building is shown in Figure 4b. Notably, the geomean spectra has SA values that are well below the lowest earthquake ground motion intensity considered in this study, corresponding to a return period of 72 years. The mean peak roof acceleration and displacement response of the Chevron building are 0.18g and 0.11m respectively. When applied in the nonlinear analysis model of the 1973 archetype, the same Loma Prieta ground motion resulted in roof accelerations and displacements of 0.20g and 0.13m, respectively. The results indicate that the mean response of the 1973 archetype is comparable to the measured response of the Chevron building. Inspection of the Chevron Building following the Loma Prieta earthquake did not reveal any damage [33], which is consistent with the analysis results of the 1973 archetype, whose response under the Loma Prieta ground motion is linear elastic.

BUILDING PERFORMANCE MODEL

In addition to direct economic losses, indirect economic losses due to downtime are significant both for building owners and the community at large. Defined as the time required to achieve a recovery state after an earthquake, downtime to re-occupancy and functional recovery are considered in this study. Re-occupancy occurs when the building is deemed safe enough to be used for shelter or minimal operations; and functional recovery occurs when the building regains its primary function, i.e. it is operational [34]. In this study, losses are calculated following the FEMA P58 methodology [10] and downtime is determined following the REDi downtime assessment methodology [35].

Loss Assessment

Owners, insurers and financial institutions often use quantitative statements of probable building repair cost expressed as a percentage of building replacement value. For time-based assessments, future repair costs can be converted to present dollars based on an assumed discount rate. Repair costs are expressed as a percentage of building replacement cost, which is estimated as \$465M based on the gross square footage with an assumed unit cost of \$3,550/m^2 (\$330/ft^2) [4]. At each earthquake ground motion intensity level considered in the MSA, one thousand loss simulations are calculated. For each realization, the losses are calculated as follows: (i) engineering demand parameters, e.g. peak story drifts and accelerations, are estimated from the results of nonlinear dynamic analyses; (ii) damage functions are used in conjunction with engineering demand parameters to determine the associated damage state for each component (structural and non-structural); (iii) consequence functions are then used to translate damage states into repair costs and repair times [10]. The direct economic losses for each realization are then estimated by conducting this calculation for every component at every story throughout the building.

Structural component quantities are based on the structural framing of the archetype buildings. Non-structural component quantities are estimated based on typical quantities found in buildings of similar occupancy using the FEMA P58 Normative Quantity Estimation Tool [10]. The components are assumed to be the same for the two archetypes considered, except that the fragilities are adjusted to account for differences in seismic design requirements of structural and non-structural components. These adjustments are based on variations in FEMA P58 damage functions based on seismic design categories. Non-structural components consistent with seismic design category D are selected for the 2015 archetype (consistent with the design of the structure), whereas non-seismically rated components are selected for the 1973 archetype (as there was no consideration of seismic design of non-structural components in the 1970s building codes). The FEMA P58 damage function library also includes variations of a same component, e.g. beam-to-column connection, to account for significant changes in design and construction practice, i.e. pre- and post-Northridge moment connection detailing, as previously illustrated in Figure 5.

The damage and repair costs are calculated using the software, SP3 [36], which employs the FEMA P58 methodology and component damage and loss functions. Excessive residual story drifts are considered through a fragility function with a median value of 1% and a dispersion of 0.3 [10] to account for cases where the building is assumed to be damaged beyond repair. Similarly, total loss due to building collapse is considered through a collapse fragility, developed from the nonlinear dynamic analysis results.

Downtime Assessment

Downtime estimates follow on from the loss estimates through the introduction of repair classes, which are assigned to the each damage state of each building component to define whether the damage level hinders achieving a certain recovery state. If the damage in any component hinders achieving a certain recovery state, the component needs to be repaired before such recovery state can be achieved.

The methodology includes a logical approach for labor allocation and repair sequencing of structural and non-structural components on a floor-per-floor basis, which accounts for contractor resource limitation and scheduling constraints. In addition to identifying the components that need repairing in order to achieve a certain recovery state, the methodology includes delay estimates associated with impeding factors, which may delay the initiation of repairs, such as the time required for post-earthquake inspection, engineering and contractor mobilization, permitting and financing. While utility disruption is also considered as part of the downtime model, in this study, it is assumed to not control over other impeding factors. In the event of irreparable damage or collapse, downtime is taken as the building replacement time, which is estimated as 1000 days based on 300 days for demolition and re-design, and 700 days for reconstruction (approximately two weeks per story).

The downtime methodology implemented in this study presents some variations over those presented in [36] including: (i) Monte Carlo simulation of downtime estimates (one downtime realization per loss realization as opposed to a single downtime realization for the median loss realization); (ii) impeding factor delays associated with contractor mobilization are weighted according to the percentage of floors in the building with damage that hinders achieving a recovery state (this is intended to account for the fact that mobilizing a team to conduct repairs in a limited number of floors within a high rise building will have a faster turnaround than mobilizing a team to conduct repairs throughout the entire building); (iii) impending factors associated with financing are only triggered when repairable damage exceeds 10% of the building replacement costs (this is intended to account for the fact that at lower damage levels building owners can finance their own repairs).

Model Parameters

A summary of the building performance model for both archetype buildings is documented in more detail in [37], including the structural and non-structural components adopted in each model, their fragility numbers (unique identifiers), component category (e.g. structure, façade, MEP, fitouts, etc.), engineering demand parameters, units, quantities and distribution of components throughout the building, as well as a summary of damage and consequence data. A summary of repair classes associated with each damage state for each building component, impeding factor delays, labor allocation parameters and utility disruption estimates associated with the downtime assessment are also included in [37].

RISK-BASED ASSESSMENT

The risk-based assessment includes calculation of the following performance metrics: (i) annual rates of collapse, λ_c, (ii) average annual losses (AAL), and (iii) average annual downtime (AAD). Additionally, loss and downtime vulnerability functions are proposed for both archetype buildings to facilitate rapid loss and downtime evaluations for regional and/or building portfolio risk assessments. Because these functions are developed based on site specific seismic hazard data, they may require adjustments when extrapolated across sites.

To provide improved resolution in the risk-based assessment, the MSA ground motion intensities summarized in Table 2 where augmented with the additional intensity levels summarized in Table 3. For these additional intensities, the structures are evaluated by scaling the ground motion sets from the original stripe levels, by the scale factors shown in Table 3. For the 1973 archetype, additional assessment levels are included for the low SA levels to better capture the onset of nonlinearity in the building. As reported in Table 3, assessment levels e_{1A}, e_{2A} and e_{3A} are introduced at

the mid-points of intervals e_1-e_2, e_2-e_3 and e_3-e_4, respectively, by scaling up the motions from the e_1, e_2 and e_3 intensities. For the 2015 archetype, additional assessment points are included to capture structural collapse at higher SA levels (e_{8A}, e_{8B} and e_{8C}) by scaling the e_8 intensity set.

Table 3. Seismic hazard data for additional intensity levels considered in the risk-based assessment including SA at a 5 second period, AFE, return period, baseline assessment point and associated scale factor.

Additional Assessment Intensity	Archetype	SA (g)	AFE (1/year)	Return Period (years)	Baseline Assessment Point	Scale Factor
e_{1A}	1973	0.07	0.0082	122	e_1	1.56
e_{2A}	1973	0.11	0.0036	278	e_2	1.29
e_{3A}	1973	0.16	0.0019	526	e_3	1.16
e_{8A}	2015	0.46	0.00016	6342	e_8	1.25
e_{8B}	2015	0.56	0.00007	14276	e_8	1.50
e_{8C}	2015	0.65	0.00005	20577	e_8	1.75

Collapse

The structural collapse risk is determined by integrating a collapse fragility function with the seismic hazard curve for the building site. Structural collapse is defined by sidesway instabilities associated with excessive lateral drifts in one or more stories, due to localization of drifts caused by a combination of p-delta and structural strength and stiffness deterioration. This is the sort of collapse behavior that has been observed in shake table studies to help validate the nonlinear analysis method [38]. The collapse fragility is described by a lognormal cumulative probability distribution that is fit to collapse data from nonlinear dynamic analyses, performed at various intensity levels ('stripes') using suites of hazard consistent ground motions at increasing shaking intensity levels. At each ground motion intensity level (or stripe in the MSA), the fraction of ground motions that cause sidesway collapse are recorded, and a lognormal cumulative probability distribution is fit to the data using the maximum likelihood method [39].

Results of the MSA dynamic analyses are shown in Figure 7a, where the peak story drift data for ground motions at each stripe level are plotted versus the SA intensity, and story drifts in excess of 0.1 indicate simulations where sidesway collapse is observed. The collapse mechanisms observed are consistent with those reported in [40], where plastic hinges form at the top of all columns in an upper story, at the bottom of all columns in a lower story, and at both ends of all beams in the intermediate stories, as illustrated in Figure 8. The resulting collapse fragilities of the two archetypes are shown in Figure 7b, where the 1973 archetype fragility has an estimated median of 0.13g and a dispersion of 0.37 and the 2015 archetype has a median of 0.54g and a dispersion of 0.28. The collapse fragility of the 1973 archetype is similar to that reported by [41] for a similar 40 story steel MRF from the 1970s. As a point of reference, the 2015 IBC [7] MCE spectral ordinate for the San Francisco building site used for the building design is approximately 0.18g for a period of T=5 seconds, corresponding to a mean annual return period of about 700 years, due to the deterministic cap applied in the MCE calculation. Thus, at the MCE intensity, the 2015 archetype has a negligible probability of collapse. In contrast, the 1973 archetype has about an 80% probability of collapse at the MCE intensity. At shorter periods (e.g. T=1 second), the return period of the MCE spectral ordinate is approximately 1100 years, consistent with that reported by SEONC's Seismology Subcommittee on Ground Motions [42].

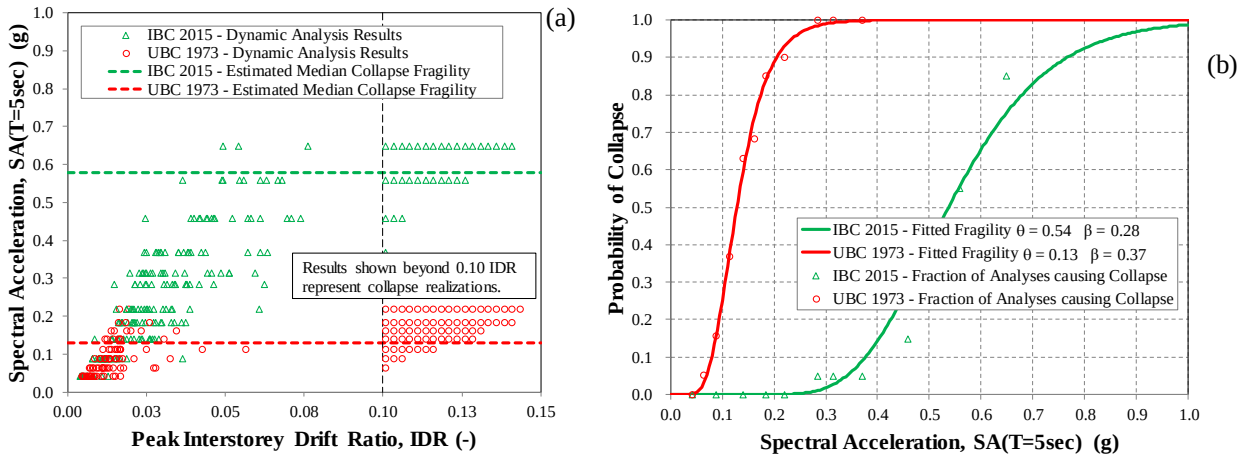

Figure 7. Collapse fragility data for the 2015 and 1973 archetype buildings: (a) Multiple Stripe Analysis (MSA) results and (b) cumulative probability distributions.

The mean annual frequency of collapse is obtained by combining the collapse fragility with seismic hazard data, which describes the mean annual frequency of exceeding the ground motion intensity. The mean annual frequency of collapse λ_c is calculated as follows:

$$\boldsymbol{\lambda_c = \int_0^\infty P(C|e) \cdot |d\lambda(e)| = \int_0^\infty P(C|e) \cdot \left|\frac{d\lambda(e)}{de}\right| \cdot de = \sum_{i=1}^{n} P(C|e_i) \cdot \left|\frac{d\lambda(e_i)}{de}\right| \cdot \Delta ei} \quad (2)$$

where P(C|e) is the probability of collapse when subjected to an earthquake with a ground motion intensity e and $\lambda(e)$ is the mean annual frequency of exceedance of the ground motion intensity e, which is an output of PSHA. The integral is typically obtained using numerical integration by multiplying the probability of collapse $P(C|e_i)$ and the slope of the seismic hazard curve at each intensity level, $|d\lambda(e_i)/de_i|$, then multiplying by the range of Δe_i (representing each intensity level), and adding the results of all intensity levels, n. This method of computing the collapse risk is outlined in more detail in [43]. Following this calculation, λ_c of the 1973 and 2015 archetypes are 28×10^{-4} and 1×10^{-4}, respectively, indicating that the annualized collapse risk of the 1973 archetype is 28 times greater than that of the 2015 archetype. The results for the 2015 archetype is also in the range of λ_c risk values of 0.7×10^{-4} to 7.0×10^{-4} calculated by [44] for modern, code-conforming RC moment frames; and 1973 steel archetype is about 20% to 60% of the λ_c risk values of 50×10^{-4} to 140×10^{-4} calculated by [45] for non-ductile RC moment frames. Nevertheless, the computed rate of collapse of the 1973 archetype is believed to exceed acceptable limits, particularly if considering the consequences associated with the collapse of a tall (50-story) building versus low and mid-rise construction (as considered in [45]).

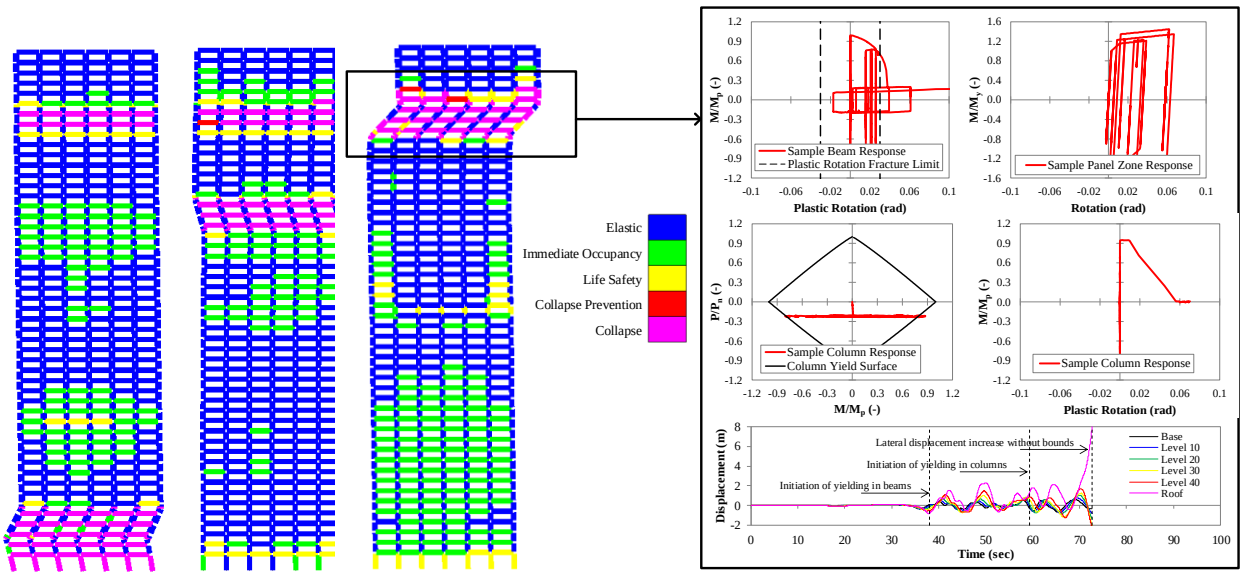

Figure 8. Contour plot illustrating ASCE 41 [29] rotation performance levels for different collapse realizations of the 1973 archetype, as well as time history data and hysteretic response of a beam, panel zone and column for a sample collapse realization.

Assuming that the collapse occurrence follows a Poisson process, the mean annual frequency of collapse can be expressed as probability of collapse in 50 years. This conversion yields a 13% probability of collapse in 50 years for the 1973 archetype and 0.5% for the 2015 archetype. In contrast, ASCE 7 [11] has a maximum risk target of 1% probability of collapse in 50 years when determining spectral values for use in design [43]. Thus, the 1973 archetype has a risk about 13 times larger than the 1% in 50 year target, while the 2015 archetype risk is about half of the target.

Losses and Downtime

The financial resources needed to recover from seismic damage to tall buildings can be significant, and thus the ability to realistically model losses is important. In order to provide a simple tool to enable estimation of expected losses for the archetype buildings considered, seismic vulnerability functions are constructed in Figures 9, 10 and 11. Vulnerability functions are frequently used in catastrophe modelling to estimate expected seismic losses to portfolios of buildings. These functions describe the expected consequence ratio (expected loss over total building cost in Figure 9, and expected downtime over total building replacement time in Figures 10 and 11) against the spectral acceleration at the fundamental period of the structure for each intensity of ground motion shaking considered in the assessment considering contributions from repairable damage, irrepairable damage and collapse.

Similar to the annualized collapse risk, the MSA results can be used to determine the average annual loss (AAL) and average annual downtime (AAD). AAL is a useful metric to evaluate annual insurance payments, and the AAD can be a useful for estimating business disruption and other indirect losses associated with building closures due to seismic damage. The AAL and AAD parameters can be determined using the loss and downtime functions, respectively, were the resulting annualized value is calculated as follows, illustrated here for AAL:

$$\boldsymbol{P(L>x) = \int P(L>x|E=e)\cdot|d\lambda(e)| = \sum_{i=1}^{n} P(L>x|e_i)\cdot\left|\frac{d\lambda(e_i)}{de}\right|\cdot \Delta ei} \quad (3)$$

$$\boldsymbol{AAL = \sum_{i=1}^{n}(L_i\cdot \Delta\lambda_i)} \quad (4)$$

Where P(L>x | E=e), the probability of exceeding a certain value of loss at a given intensity of ground motion shaking, is integrated with the seismic hazard curve |dλ(e)|, shown previously in Figure 4. As shown in Figure 9, the loss function P(L>x | E=e) is aggregated from three components, corresponding to: (1) Collapse, (2) Non-collapse, non-repairable damage, and (3) Non-collapse, repairable damage. As with the collapse risk estimation, the integral shown in equation 3 can be solved through numerical integration over the number of earthquake ground motion intensities,

n, considered in the risk-based assessment, where intensity e_i is assumed to represent all earthquake ground motion shaking intensities in the interval Δe_i. In Equation 4, $\Delta\lambda_i$ is the annual rate of occurrence of intensity level i.

The resulting AALs, reported in terms of normalized building replacement value, are shown in Figure 9, where the pie charts show the relative contributions of collapse, demolition and repair to the total loss. The total AALs for the 1973 and 2015 archetype buildings are 0.66% and 0.40%, respectively, of building replacement cost, where in rather stark contrast to the large difference in collapse risks, the losses are only about 1.65 times larger for the 1973 archetype. The estimated AAD to re-occupancy, shown in Figure 10, is 8.1 days for the 1973 archetype versus 4.7 days for the 2015 archetype; and the AADs to functional recovery, shown in Figure 11, are 10.4 days and 5.0 days, respectively. These annualized downtime metrics follow similar patterns to the corresponding AALs, including the relative contributions of collapse and irreparable damage. Referring to the pie charts in Figures 9, 10 and 11, the collapse risk is the greatest contributor to the expected losses in the 1973 archetype, whereas residual story drifts rendering the building irreparable are the greatest contributor to loss in the 2015 archetype. Given the likelihood of observing collapse or demolition and their implications on cost and downtime (total replacement cost and time, i.e. a loss or downtime ratio of 1.0), it is important that these are considered when computing the AAL and the AAD. As a reference point, [46] evaluated the performance of a set of modern RC frame 20-story buildings to have AALs on the order of 0.46% to 0.70% of building replacement cost. Similarly, [47] evaluated the AAL of modern steel MRF 20-story buildings to range from 0.43% to 0.53%. These results are consistent with the results for the 2015 steel building archetype.

While annualized loss and downtime metrics are useful for risk management and recovery planning, they are not as intuitive as an intensity based assessment. For reference, the intensity levels closest to the ASCE 7 [11] MCE spectral ordinate (equal to 0.18g for T=5-second period), the DBE spectral ordinate (defined as two-thirds of MCE, equal to 0.12g) and the 1989 Loma Prieta ground motion measured at the Chevron Building [33] are indicated in Figures 9, 10 and 11. At the intensity level closest to DBE shaking (intensity level e_{2A}), the 1973 archetype has an expected loss ratio of 0.58 (i.e. $270M), and expected downtime ratios of 0.65 (i.e. 650 days) to re-occupancy and 0.67 (i.e. 670 days) to functional recovery. These estimates are based on a 50% probability of observing repairable damage, 14% of demolition and 36% of collapse. In contrast, the 2015 archetype has an expected loss ratio of 0.11 (i.e. $51M), and expected downtime ratio of 0.15 (i.e. 150 days) and 0.18 (i.e. 180 days) to re-occupancy and functional recovery, respectively. These estimates are based on a 95% probability of observing repairable damage and 5% of demolition.

At the intensity level closest to MCE shaking (intensity level e_4), the 1973 archetype has an expected loss ratio of 0.91 (i.e. $423M), and expected downtime ratio of 0.92 (i.e. 920 days) and 0.93 (i.e. 930 days) to re-occupancy and functional recovery, respectively. These estimates are based on a 12% probability of observing repairable damage, 4% of demolition and 84% of collapse. In contrast, the 2015 archetype has an expected loss ratio of 0.22 (i.e. $103M), and expected downtime ratios of 0.37 (i.e. 370 days) and 0.40 (i.e. 400 days) to re-occupancy and functional recovery, respectively. These estimates are based on a 87% probability of observing repairable damage and 13% of demolition.

Loss deaggregation of repairable damage at DBE and MCE shaking is illustrated in Figure 12a for both archetype buildings, including contributions from structure, fitouts, façade, egress and MEP components throughout the building. The results indicate that façade damage is the greatest contributor to losses in the 1973 archetype, whereas office fitouts are the largest contributor to the 2015 archetype. This difference is due to a combination of factors, including higher drifts and a more fragile façade fragility function in the 1973 archetype. Deaggregations of downtime to re-occupancy and functional recovery for realizations in which building damage is repairable are illustrated in Figures 12b and 12c, respectively. The results, which highlight contributions from structural repairs, non-structural repairs and impeding factor delays, indicate that non-structural repairs and impeding factor delays are the greatest downtime contributors.

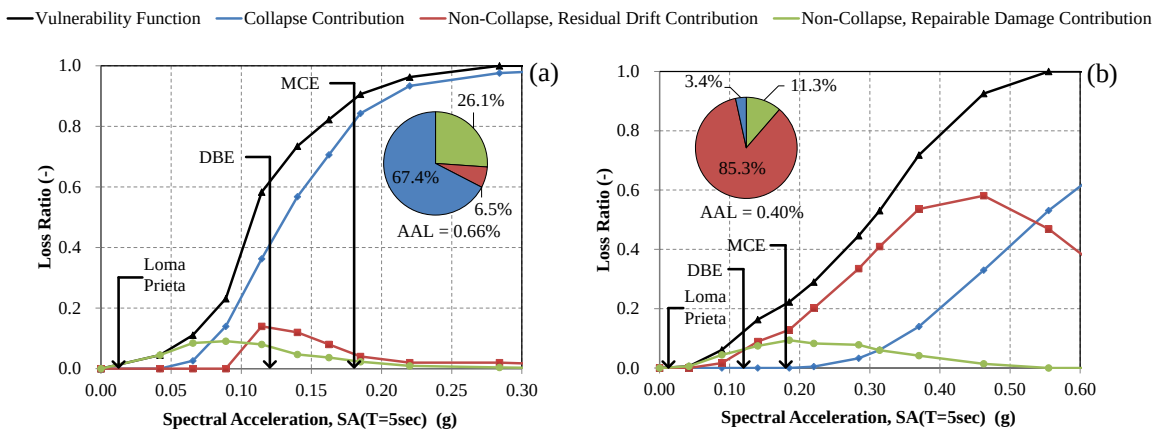

Figure 9. Loss vulnerability function and associated average annual loss (AAL) for the (a) 1973 and (b) 2015 buildings including contributions from collapse, irreparable damage and repairable damage.

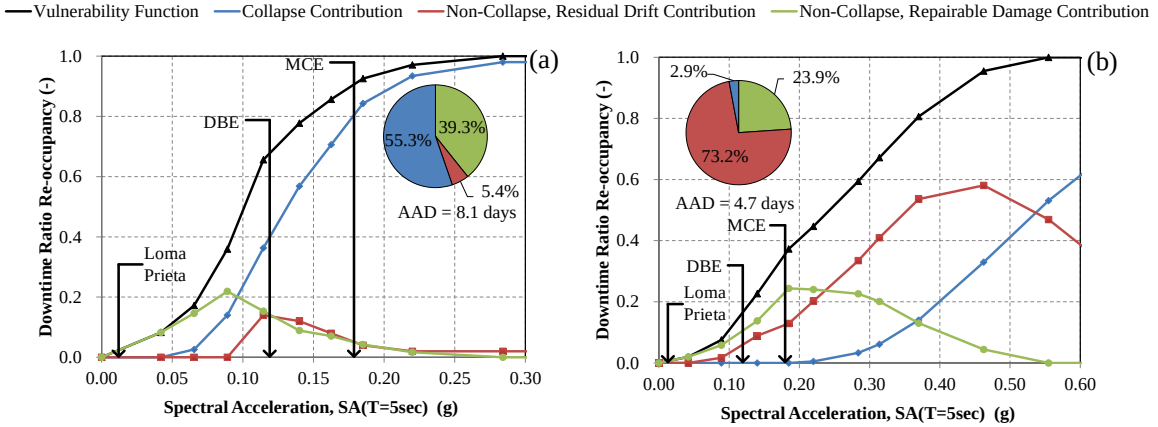

Figure 10. Downtime to re-occupancy vulnerability function and associated average annual downtime (AAD) for the (a) 1973 and (b) 2015 buildings including contributions from collapse, irreparable damage and repairable damage.

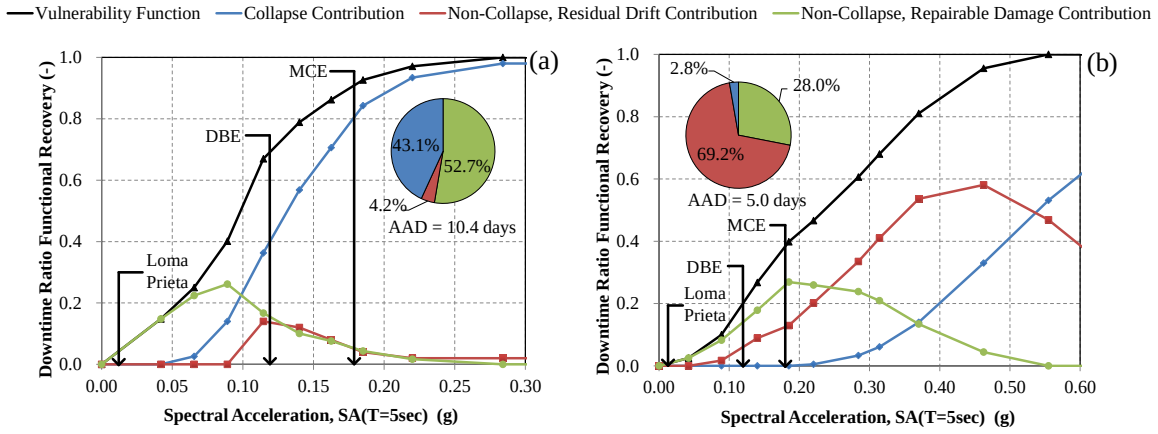

Figure 11. Downtime to functional recovery vulnerability function and associated average annual downtime (AAD) for the (a) 1973 and (b) 2015 buildings including contributions from collapse, irreparable damage and repairable damage.

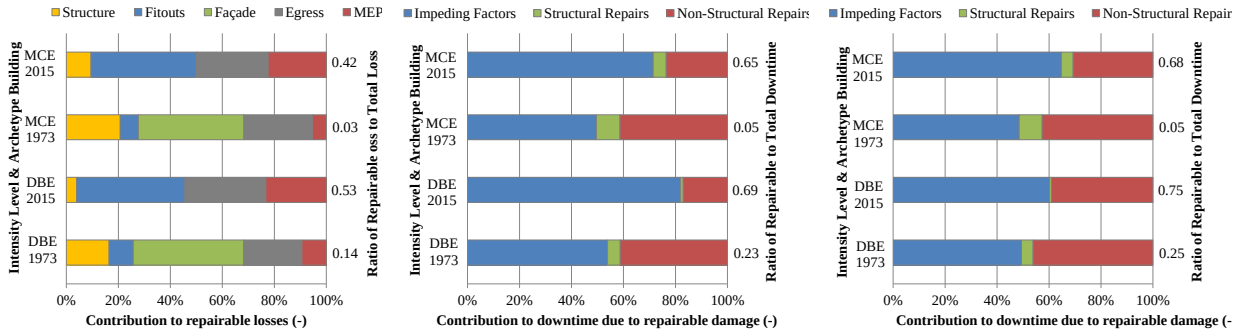

(a) (b) (c)

Figure 12. Deaggregation of (a) repairable loss, (b) downtime to re-occupancy, and (c) downtime to functional recovery for the 1973 and 2015 archetype buildings at intensity levels closest to DBE and MCE shaking.

CONCLUSIONS

This study benchmarks the performance of older existing tall steel MRF buildings designed following historic code-prescriptive requirements (UBC 1973) against modern design standards (IBC 2015) by means of risk-based assessments of alternative designs of a 50-story archetype office building, located at a site in San Francisco, CA. The comparison focuses on risk metrics including annualized rates of collapse, economic loss and downtime. Furthermore, an evaluation of the results at code defined DBE and MCE earthquake ground motion shaking intensities is also provided. The main findings of this study can be summarized as follows:

- The mean annual frequency collapse risk of the 1973 archetype building is 28 times greater than the equivalent 2015 building (28×10^{-4} versus 1×10^{-4}), or approximately 13% versus 0.5% probability of collapse in 50 years. The collapse risk of the modern archetype is well within the 1% in 50 year target of modern codes. The 1973 archetype has a probability of collapse about 13 times larger than the code target. However, its collapse risk is only a fraction (in the range of 20-60%) of that calculated by other researchers [43] for non-ductile RC moment frames. In order to ensure a holistic comparison, when using annual frequency of collapse as a metric to contrast risks across vulnerable building taxonomies, care must be taken to consider the broader consequences of failure, e.g. collapse of a 50-story building vs low and mid-rise construction (as considered in [43]).
- The average annual economic loss is 65% higher for the 1973 as compared to the 2015 building (0.66% versus 0.40% of building replacement cost). The average annual downtime to re-occupancy for the 1973 building is about 72% longer (8.1 vs 4.7 days) and to functional recovery is about 100% longer (10.4 vs 5.0 days). While annualized loss and downtime estimates are considerably larger for the 1973 as compared to the 2015 archetype, the differences are drastically less staggering than the corresponding collapse risks. Smaller differences in loss and downtime metrics are a result of two distinct performance levels, demolition vs collapse, having a common outcome, total building replacement cost and time, within the loss and downtime assessment framework. Annualized losses and downtime in the 2015 archetype are dominated by risk of demolition, whereas collapse risk is the greatest contributor in the 1973 archetype. Normalized costs and time associated with repairable damage tend to be relatively low in tall buildings due to the concentration of deformations in a small number of stories, where the rest of the building may be undamaged. This puts even greater emphasis on the contributions of demolition and collapse to annualized loss and downtime metrics because building performance transitions from a low loss or downtime ratio to total building replacement due to excessive drifts in one or a few stories, which result in the building being declared a total loss and demolished. While annualized loss and downtime metrics are useful for building owners and the community at large, they may fail to provide a clear picture of the true seismic risks.
- Evaluation of results at DBE and MCE further suggest that the 1973 archetype has much higher risks of collapse under extreme ground motions, and risks of damage and building closure in moderate earthquakes. Furthermore, while modern building code requirements provide acceptable seismic collapse safety, they do not necessarily ensure a level of damage control to assure a swift recovery after a damaging earthquake due to extensive downtime.

Although results presented are based on a number of simplifying assumptions, these are applied consistently across the two archetypes considered, thereby providing valuable information of relative seismic performance between older (1970s) and modern steel MRF buildings, which can help make more informed risk-management decisions. Further research is required to extend the metrics here presented across steel moment resisting frames as a broader building taxonomy.

ACKNOWLEDGMENTS

The authors would like to thank Haselton and Baker Risk Group for providing access to SP3. The authors would also like to thank Arup for their technical support, particularly Ibbi Almufti for his advice and contributions to the study, especially the REDi components of downtime. Lastly, the authors would like to thank Risk Management Solutions for their significant contributions through research discussions, particularly for highlighting the benefit of generating vulnerability functions for older tall steel moment frame buildings and benchmarking their performance against modern design standards. Any opinions, findings, conclusions or recommendations expressed in this material are those of the authors and do not necessarily reflect those of the individuals or companies here acknowledged.

REFERENCES

[1] NZPA, "Christchurch earthquake: Cordon around Grand Chancellor narrows," www.stuff.co.nz, 2011. [Online]. Available: http://www.stuff.co.nz/national/christchurch-earthquake/4716748/Christchurch-earthquake-Cordon-around-Grand-Chancellor-narrows [Accessed 24-May-2018]

[2] FEMA, "Next generation performance based seismic design guidelines," Federal Emergency Management Agency, Rep. FEMA 445, Washington, DC, 2006.

[3] PEER, "Tall buildings initiative: Guidelines for performance-based seismic design of tall buildings," Pacific Earthquake Engineering Research Center, Rep. No. 2010/05, Univ. of California, Berkeley, CA, 2010.

[4] C. Molina Hutt, I. Almufti, G. G. Deierlein, M. Willford, "Seismic Loss and Downtime Assessment of Existing Tall Steel-Framed Buildings and Strategies for Increased Resilience," *J. Struct. Eng.*, vol. 142, no. 8, p. C4015005, 2016.

[5] Crouse C. B., Leyendecker E. V., Somerville P. G., Power M., & Silva W. J., "Development of seismic ground-motion criteria for the ASCE 7 standard," Proc. 8th US National Conference on Earthquake Engineering, San Francisco, CA, 2006.

[6] ICBO, "Uniform Building Code (UBC) 73," International Conference of Building Officials, Whittier, CA, 1973.

[7] ICC, "2015 International Building Code (IBC)," International Code Council, Country Club Hills, IL, 2015.

[8] NEHRP, "Selecting and scaling earthquake ground motions for performing response-history analyses," NIST GCR 11-917-15 prepared by NEHRP Consultants Joint Venture for the National Institute of Standards and Technology, Gaithersburg, MD, 2011.

[9] J. Moehle and G. G. Deierlein, "A framework methodology for performance-based earthquake engineering," Proc., 13th World Conf. of Earthquake Engineering, International Association for Earthquake Engineering, Tokyo, 2004.

[10] FEMA, "Seismic performance assessment of buildings," Federal Emergency Management Agency, Rep. FEMA P-58, Washington, DC, 2012.

[11] ASCE, "Minimum design loads for buildings and other structures," ASCE/Structural Engineering Institute (SEI) 7, Reston, VA, 2010.

[12] ATC, "San Francisco Tall Buildings Study," Applied Technology Council, Redwood City, CA, 2018.

730 [13] SEAOC, "Recommended lateral force requirements and commentary," Structural Engineers Association of
731 California, Sacramento, CA, 1973.
732
733 [14] P. communication, H.J. Brunnier Associates, Degenkolb Engineers, Rutherford and Chekene, San Francisco,
734 CA, 2012.
735
736 [15] FEMA, "Recommended post-earthquake evaluation and repair criteria for welded steel moment-frame
737 buildings," Federal Emergency Management Agency, Rep. FEMA 352, Washington, DC, 2000.
738
739 [16] PEER, "Modeling and acceptance criteria for seismic design and analysis of tall buildings," Pacific Earthquake
740 Engineering Research. Rep. No. 2010/111, Univ. of California, Berkeley, CA, 2010.
741
742 [17] SAC, "Performance prediction and evaluation of steel special moment frames for seismic loads," SAC Steel
743 Project, SAC Rep. No. SAC/BD-00/25, Richmond, CA, 2000.
744
745 [18] M. Bruneau and S. A. Mahin, "Ultimate behavior of heavy steel section welded splices and design
746 implications," *J. Struct. Eng.*, vol. 116, issue 8, pp. 2214, 1990.
747
748 [19] USGS, "USGS Unified Hazard Tool," USGS, 2017. [Online]. Available:
749 https://earthquake.usgs.gov/hazards/interactive/ [Accessed 24-May-2018]
750
751 [20] J. W. Baker and C. A. Cornell, "Spectral shape, epsilon and record selection," *Earthquake Engng. Struct. Dyn.*,
752 vol. 35, pp. 1077-1095, 2006.
753
754 [21] T. Lin and J. W. Baker, "Conditional Spectra," Encyclopedia of Earthquake Engineering, M. Beer, I. A.
755 Kougioumtzoglou, E. Patelli, S.-K. Au (Eds.), pp. 461-472, Springer Berlin Heidelberg, 2015.
756
757 [22] J. W. Baker and C. Lee, "An Improved Algorithm for Selecting Ground Motions to Match a Conditional
758 Spectrum," *Journal of Earthquake Engineering*, vol. 22, no. 4, pp. 708-723, 2018.
759
760 [23] E. H. Field, T. H. Jordan and C. A. Cornell, "OpenSHA: A Developing Community-Modeling Environment for
761 Seismic Hazard Analysis," *Seismological Research Letters*, vol. 74, no. 4, pp. 406-419, 2003.
762
763 [24] PEER, "PEER NGA-West2 Database," Pacific Earthquake Engineering Research Center, Rep. No. 2013/03,
764 Univ. of California, Berkeley, CA, 2013.
765
766 [25] T. Lin and J. W. Baker, "Conditional spectrum-based ground motion selection. Part I: Hazard consistency for
767 risk-based assessments," *Earthquake Engng Struct. Dyn.*, vol. 42, no. 12, pp. 1847-1865, 2013.
768
769 [26] LSTC, LS-DYNA 971 [Computer software], Livermore Software Technology Corporation, Livermore, CA.
770
771 [27] D. G. Lignos and H. Krawinkler, "Deterioration Modeling of Steel Components in Support of Collapse
772 Prediction of Steel Moment Frames under Earthquake Loading," *J. Struct. Eng.*, vol. 137, no. 11, pp. 1291-1302,
773 2011.
774
775 [28] N. Al-Shawwa and D. G. Lignos, "Web-Based Interactive Tools for Performance-Based Earthquake
776 Engineering," McGill University, 2013. [Online]. Available: http://dimitrios-lignos.research.mcgill.ca/databases/
777 [Accessed 24-May-2018]
778
779 [29] ASCE, "Seismic Evaluation and Retrofit of Existing Buildings," ASCE/Structural Engineering Institute (SEI)
780 41, Reston, VA, 2013.
781
782 [30] M. Kurata, K. Suita and M. Nakashima, “Test on large cyclic deformation of steel tube columns having fixed
783 column bases,” *J. Struct. Constr. Eng.* (in Japanese), vol. 598, pp. 149–154, 2005.
784
785 [31] D. G. Lignos and H. Krawinkler, "A steel database for component deterioration of tubular hollow square steel

columns under varying axial load for collapse assessment of steel structures under earthquakes," in Proc., 7th Int. Conf. on Urban Earthquake Engineering and 5th Int. Conf. on Earthquake Engineering, Tokyo, 2010.

[32] CESMD, "Strong Motion Center," Center of Engineering Strong Motion Data," 2003. [Online]. Available: http://www.strongmotioncenter.org/ [Accessed 24-May-2018]

[33] J. C. Anderson and V. V. Bertero, "Seismic response of a 42-story steel building," United States Geological Survey, Professional Paper 1552-C, Washington, DC, 1998.

[34] D. Bonowitz, "Resilience Criteria for Seismic Evaluation of Existing Buildings," Structural Engineers Association of Northern California, Special Projects Initiative Report, San Francisco, CA, 2011.

[35] I. Almufti and M. Wilford, "Resilience-based Earthquake Design Initiative (REDi) for the Next Generation of Buildings," Arup, San Francisco, CA, 2013.

[36] SP3, Seismic Performance Prediction Program [Computer Software], Haselton Baker Risk Group, Chico, CA.

[37] C. Molina Hutt, "Risk-based seismic performance assessment of existing tall steel framed buildings," Ph.D. Dissertation, University College London (UCL), London, UK, 2017.

[38] D. G. Lignos, Y. Chung, T. Nagae, M. Nakashima, "Numerical and Experimental Evaluation of Seismic Capacity of High-Rise Steel Buildings Subjected to Long Duration Earthquakes," *Journal of Computers and Structures*, vol. 89, no. 11-12, pp. 959-967, 2011.

[39] J. Baker, "Efficient analytical fragility function fitting using dynamic structural analysis," *Earthquake Spectra*, vol. 31, no. 1, 2015.

[40] S. Krishnan and M. Muto, "Mechanism of collapse of tall steel moment frame buildings under earthquake excitation," Proc., 15th World Conf. of Earthquake Engineering, International Association for Earthquake Engineering, Lisbon, Portugal, 2012.

[41] C. Molina Hutt, I. Almufti , M. Willford and G. G. Deierlein, "Risk-based seismic performance assessment of existing tall steel-framed buildings in San Francisco," Proc., SECED 2015 Conference: Earthquake Risk and Engineering towards a Resilient World, Cambridge, UK, 2015.

[42] SEAONC, "2475-year ground motion? Not in coastal California!" Structural Engineers Association of Northern California, 2009. [Online]. Available: https://seaonc.org/sites/default/files/newsletter-archive/aug09.pdf [Accessed 24-May-2018]

[43] L. Eads, "Seismic collapse risk assessment of buildings: effects of intensity measure selection and computational approach," Stanford University, Civil & Environmental Engineering Department., Stanford, CA, 2013.

[44] C. B. Haselton and G. G. Deierlein,"Assessing Seismic Collapse Safety of Modern Reinforced Concrete Frame Buildings," Pacific Engineering Research Center, PEER Report 2007/08, University of California, Berkeley, CA. 2007.

[45] A. B. Liel, C. B. Haselton and G. G. Deierlein, "Seismic Collapse Safety of Reinforced Concrete Buildings. II: Comparative Assessment of Nonductile and Ductile Moment Frames," *J. Struct. Eng.*, vol. 137, no. 4, pp. 492-502, 2011.

[46] C. M. Ramirez, A. B. Liel, J. Mitrani-Reiser, C. B. Haselton, A. D. Spear, J. Steiner, G. G. Deierlein and E. Miranda, "Expected earthquake damage and repair costs in reinforced concrete frame buildings.," *Earthquake Engng Struct. Dyn.*, vol. 41, no. 11, pp. 145, 2012.

[47] S. H. Hwang and D. G. Lignos, "Earthquake-induced loss assessment of steel frame buildings with special

882 moment frames designed in highly seismic regions." *Earthquake Engng Struct. Dyn*., vol. 46, pp. 2141-2162 , 2017.